

H I Mapping of Galaxies in six GEMS Groups^{*}

Katie M. Kern^{1,2}, Virginia A. Kilborn^{1,2}, Duncan A. Forbes¹ and Bärbel Koribalski²

¹Centre for Astrophysics & Supercomputing, Swinburne University of Technology, Hawthorn, VIC 3122, Australia

²Australia Telescope National Facility, CSIRO, P.O. Box 76, Epping, NSW 1710, Australia

Received date; accepted date

ABSTRACT

Here we present Australia Telescope Compact Array H I maps of 16 H I sources in six Group Evolution Multiwavelength Study (GEMS) groups that were previously observed with the Parkes telescope. The higher spatial resolution of the ATCA allows us to clearly identify the optical counterparts for the first time – most being associated with low surface brightness late-type galaxies. New integrated H I maps and velocity fields for each source are presented. We find several interacting systems; one of which contains three galaxies within a common H I envelope. Extended H I structures in the sample are more consistent with tidal effects than ram pressure stripping. We identify two H I detections with previously uncatalogued optical galaxies, and add a total of six newly identified group members to the NGC 3923, 5044 and 7144 groups.

Key words: surveys, radio lines - galaxies: cluster: general - galaxies: evolution - galaxies: irregular

1 INTRODUCTION

Approximately half of all galaxies reside in galaxy groups (Eke et al. 2004). Despite being so abundant in the universe, the properties of groups and their constituent galaxies have been less well studied compared to rare galaxy clusters. Most detailed multiwavelength studies to date (e.g. Mulchaey & Zabludoff 1998) have been restricted to a small number of groups.

Galaxies in the dense environments of cluster cores exhibit suppressed star formation rates, neutral hydrogen (H I) deficiencies, bulge-dominated morphologies, and redder colors than their field counterparts (e.g. Wilman et al. 2005a,b). The environment of galaxy groups is also thought to have a strong impact on the evolution of constituent galaxies. It has been argued to be the most effective environment for galaxy interactions and mergers due to the low relative velocities in groups (e.g. Mulchaey & Zabludoff 1998; Mamon 2006). Given these low velocities, and low intragroup gas densities, it is expected that ram pressure stripping plays a much reduced role in groups compared to clusters, however examples do exist (e.g. Rasmussen, Ponman & Mulchaey 2006).

H I mapping is an extremely useful technique in understanding galaxy groups, as most H I envelopes around galaxies tend to extend further out than the stellar component,

and as such, are the first component of the galaxies to react to external forces (Broeils & van Woerden 1994). Therefore, the H I properties of group galaxies serve as a sensitive indicator of past and present interactions, as well as internal kinematics, mass, and orientation parameters of the galaxies themselves. Several studies of H I in galaxy groups have been made, showing that group galaxies often display H I material that is extended and stripped away from their host galaxies (e.g. Gordon et al. 2003; Kantharina et al. 2005; Koribalski & Manthey 2005; Kilborn et al. 2006). In the case of compact groups, galaxies in such environments appear to be deficient in H I (Verdes-Montenegro et al. 2001) but see Stevens et al. (2004) for a different view point.

To gain a better understanding of the processes operating within groups, the Group Evolution Multiwavelength Study (GEMS) was established. For details of the selection criteria and science goals, see Osmond & Ponman (2004) and Forbes et al. (2006). Briefly, this is a multiwavelength study of 60 nearby galaxy groups, using X-ray, optical, infrared and H I data. All have deep ROSAT X-ray maps available. We have also obtained wide-field H I observations of 16 southern GEMS groups using the multibeam receiver on the Parkes Radio telescope (Kilborn et al. 2007). This Parkes survey, which is about twice as sensitive as the HIPASS survey (Barnes et al. 2001), has discovered several new galaxy group members (McKay et al. 2004; Kilborn et al. 2005) and interesting cases of extended H I gas (Kilborn et al. 2007). In the Kilborn et al. (2007) survey there are ~ 50 sources for which the H I detection could not be confidently assigned to a single (optical) galaxy. This ‘confusion’ is due to the

^{*} The observations were obtained with the Australia Telescope Compact Array which is funded by the Commonwealth of Australia for operations as a National Facility managed by CSIRO.

relatively large beamsize of the Parkes telescope, i.e. 15.5'. Here we report the first of our higher resolution (beamsize $\sim 2'$) H I maps with the Australian Telescope Compact Array (ATCA) of 16 confused sources in six GEMS groups. Our aim is to identify the correct optical counterpart and map the H I at higher spatial resolution.

2 OBSERVATIONS AND DATA REDUCTION

Our H I line observations of 16 Parkes sources were obtained with the ATCA in ‘snapshot’ mode over several observing runs in 2004 March, 2004 June, 2004 November, 2005 January, and 2006 January. Data were obtained using various configurations of the 750 array, and an 8 MHz bandwidth with 512 channels. The observing parameters, such as the array used, date of observations, integration time per source, phase calibrator, and central observing frequency for the sixteen sources can be found in Table 1. The primary calibrator used for all sources was PKS 1934-638, and the secondary calibrator was generally kept the same for individual galaxy groups.

Also listed in Table 1 are the deconvolved beamsizes for each field, and the noise as measured from the cleaned channel maps near the H I emission using MIRIAD task CGDISP. The H I column density limit is calculated using Equation 1 at a detection level of 3σ . The H I mass sensitivity, calculated by Equation 2, is the lower H I mass limit detectable for each source, assuming a distance D to each group from Brough et al. (2006) and an integrated H I flux of width $W = 100 \text{ km s}^{-1}$ at the 3σ level (in mJy beam^{-1}). In the best case we have a sensitivity of $\sim 10^8 M_{\odot}$.

$$N_{\text{H I}} = \frac{1.82 \times 10^{18} \times 3\sigma \times 685}{\text{beamsize} \times 1.2} \text{ atoms cm}^{-2} \quad (1)$$

$$\text{Sensitivity} = 2.36 \times 10^2 \times D^2 \times 3\sigma \times W \text{ } M_{\odot} \quad (2)$$

The data were reduced using standard MIRIAD routines including flagging, bandpass calibration, subtraction of the continuum, and inverted into the real domain. The final H I cubes were made using natural weighting and smoothed to a velocity resolution of 6.6 km s^{-1} . The channels were cleaned, giving an rms noise of $\sim 1\text{-}2 \text{ mJy beam}^{-1}$. The resulting H I moment maps for the detections were prepared using the MIRIAD task MOMENT, where each map was masked to the lowest H I integrated intensity contour using MATHS (for most galaxies, the lowest contour was 0.5 Jy beam^{-1}).

The integrated intensity maps were run through IMFIT to determine the position of the galaxies, whereby this central position was used in MBSPECT with the H I cubes to measure the central H I velocity and the width of the line profile at the 50% peak flux density W_{50} . To determine the total integrated H I flux, the task CGDISP was once again used on the integrated intensity maps, where multiple polygons were drawn around the source at varying radii to determine the mean and deviation of the integrated flux. We note that due to the relatively short exposure times in snapshot mode, the integrated fluxes are likely to be lower estimates of the true total flux and we refer the reader to Kilborn et al. (2007) for total source fluxes. Basic properties of the 19 galaxies detected in our ATCA observations are summarised in Table 2.

3 RESULTS

We observed sixteen confused Parkes H I sources in six GEMS galaxy groups from the catalogue of Kilborn et al. (2007) and identified 19 optical counterparts to these sources with the superior resolution of the ATCA. The total H I flux for these sources from the Parkes telescope are given in Kilborn et al. (2007). In Table 2 we list the ATCA H I measurements and our optical identification based on galaxies in the NASA Extragalactic Database (NED; ned-www.ipac.caltech.edu) and the Digital Sky Survey (DSS; www.gssts.stsci.edu/SkySurveys/SkySurveys.htm). For three of the Parkes sources we resolved multiple H I sources. These are denoted by A or B added to the end of the GEMS Name of the Parkes source. In each case a catalogued galaxy to the A and B H I source could be clearly identified. Of the remaining 13 Parkes sources we were able to confidently associate 11 of them with an optical counterpart based on their spatial coincidence. For two H I sources (which we refer to as GEMS_N3923_11 and GEMS_N5044_18) no previously catalogued optical galaxy could be found in the NED database, however we could clearly identify a small, low surface brightness galaxy in the DSS in both cases. For a total of six galaxies no previous redshift was catalogued. From the GEMS project (this work, Kilborn et al. 2007 and McKay et al. 2004) we find all six to have locations and redshifts consistent with group membership. Details of our results for individual galaxies are described in the next section.

3.1 NGC 1332 Group

IC 1953 This is a late-type barred spiral galaxy. The H I detected here does not extend further than the stellar component, and has peaks to either side of the nucleus (Figure 1). The galaxy to the north-east of IC 1953 (in the DSS image) is ESO 548-G040 which lies in the background at a velocity of 4061 km s^{-1} .

NGC 1385 This is a barred spiral galaxy. The H I of this galaxy is evenly distributed and extends beyond the stellar component (Figure 1). The H I velocity contours show a normal differentially rotating disk, although a slight warp appears in the outer regions. The H I spectrum is fairly symmetric, showing one central peak.

3.2 NGC 1808 Group

ESO 362-G011 This is a highly inclined Sbc spiral. The integrated H I is evenly distributed, following the position angle (P.A.) of the stellar component at 76° , and extends above and below the disk (Figure 1). There is also a slight extension of the H I distribution to the north-east and south-west. The velocity field reveals an evenly rotating galactic disk. The galaxy seen to the left of ESO 362-G011 (on the DSS image) is a background galaxy ESO 362-G012 at a velocity of 4638 km s^{-1} . The H I spectrum follows the classic double horned profile.

3.3 NGC 3923 Group

ESO 439-G025 This edge-on Sb spiral has a bright central nucleus (Figure 1). The H I follows the stellar component

Table 1. ATCA observing parameters.

GEMS Name	Beamsize [arcsec ²]	$N_{H\text{I}}$ [10^{18} cm ⁻²]	Sensitivity [$10^8 M_{\odot}$]	Noise [mJy beam ⁻¹]	Obs. Freq. [MHz]	Calibrator	Int. Time [minutes]	Array	Date
(1)	(2)	(3)	(4)	(5)	(6)	(7)	(8)	(9)	(10)
GEMS_N1332_03	150×45	2.7	1.8	6	1412	0405-385	135	750B	2005-01-17
GEMS_N1332_13	121×50	3.0	1.8	6	1412	0405-385	150	750B	2005-01-17
GEMS_N1808_01	89×47	4.5	1.2	6	1412	0405-385	140	750B	2005-01-17
GEMS_N3923_08	114×51	3.1	1.9	6	1411	1151-348	143	750C	2004-11-12
GEMS_N3923_11	101×58	2.6	1.6	5	1411	1151-348	156	750C	2004-11-12
GEMS_N3923_13	119×52	3.0	1.9	6	1411	1151-348	137	750C	2004-11-12
GEMS_N5044_01	178×46	1.9	3.0	5	1407	1245-197	270	750D	2006-01-26
GEMS_N5044_05	168×51	2.9	4.8	8	1407	1245-197	132	750D	2006-01-28
GEMS_N5044_10	221×45	1.9	3.6	6	1407	1245-197	265	750D	2006-01-27
GEMS_N5044_14	183×51	2.3	4.2	7	1407	1245-197	132	750D	2006-01-28
GEMS_N5044_18	202×47	1.9	3.6	6	1409	1245-197	265	750D	2006-01-27
GEMS_N7144_01	76×45	8.1	3.3	9	1411	2134-470	116	750D	2004-06-05
GEMS_N7144_05	75×50	2.5	1.1	3	1411	2106-413	588	750A	2004-06-04
GEMS_N7144_06	78×45	7.0	2.9	8	1411	2134-470	105	750D	2004-06-05
GEMS_N7144_07	78×52	2.3	1.1	3	1411	2106-413	639	750A	2004-06-03
GEMS_HCG90_11	90×50	4.8	6.4	7	1408	2149-306	135	750D	2004-06-05

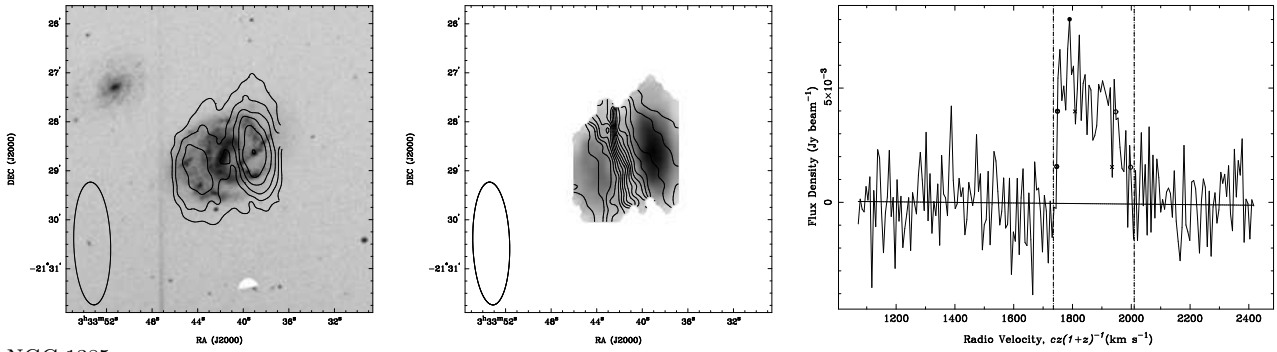
The columns are (1) GEMS name (2) beamsize, (3) column density, (4) sensitivity, (5) noise, (6) central observing frequency, (7) the phase calibrator used, (8) total integration time on the source, (9) array used, (10) the date of the observation.

Table 2. Properties of the detected GEMS galaxies.

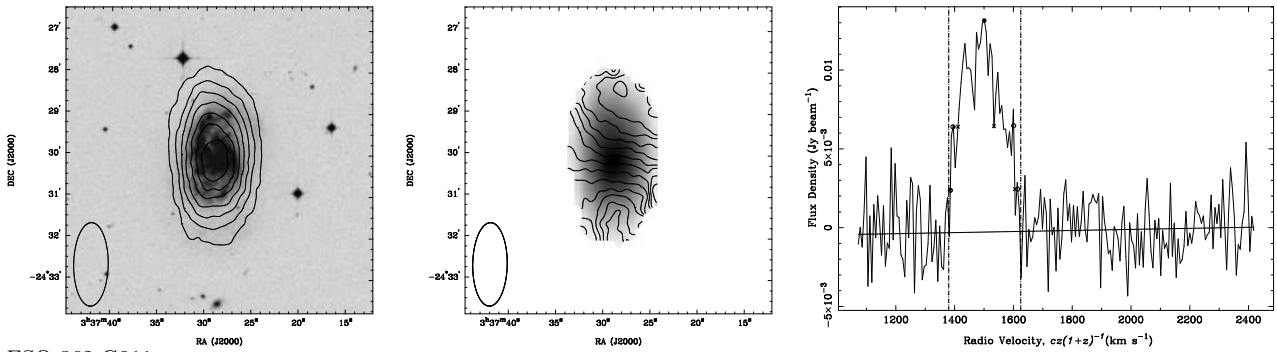
GEMS Name	Optical ID	HI position [^h ^m s], [^o ' '']	V_{HI} [km s ⁻¹]	W_{50} [km s ⁻¹]	S_{HI} [Jy km s ⁻¹]	M_{HI} $10^8 M_{\odot}$	V_{opt} [km s ⁻¹]	Type
(1)	(2)	(3)	(4)	(5)	(6)	(7)	(8)	(9)
GEMS_N1332_03	IC 1953	03:33:40.0, -21:28:39.5	1844	198	5.9±0.1	13.4±0.9	1860	SB(rs)d
GEMS_N1332_13	NGC 1385	03:37:29.0, -24:30:03.6	1492	207	17.7±0.3	21.5±1.9	1502	SB(s)cd
GEMS_N1808_01	ESO 362-G011	05:16:39.7, -37:06:09.8	1338	275	56±1	37.9±1.5	1367	Sbc
GEMS_N3923_08	ESO 439-G025	11:43:45.9, -30:37:13.8	1972	133	5.4±0.1	7.2±0.6	—	Sb
GEMS_N3923_11	—	11:50:17.2, -30:01:25.0	1594	57	0.6±0.2	1.4±0.4	—	—
GEMS_N3923_13	[KK2000] 47	11:57:30.0, -28:07:39.8	2112	35	1.7±0.1	1.8±0.3	—	Irr/Sph
GEMS_N5044_01	LEDA 083818	13:13:59.6, -16:47:28.1	3037	140	1.0±0.2	8.7±1.0	—	Sd
GEMS_N5044_05	RC3 1303.0-1530	13:05:34.0, -15:45:09.0	2875	99	1.7±0.1	7.7±1.0	—	SB(s)dm
GEMS_N5044_10	[MMB2004] J1320-1427	13:20:13.5, -14:27:36.4	2723	45	2.4±0.1	9.7±1.1	—	—
GEMS_N5044_14	RC3 1305.5-1430	13:08:06.3, -14:46:43.4	2578	106	1.5±0.5	11.1±1.1	—	IB(s)m
GEMS_N5044_18	—	13:11:33.1, -14:40:39.8	2421	72	0.3±0.1	6.3±0.9	—	—
GEMS_N7144_01A	ESO 236-G039	21:45:13.8, -49:00:32.0	1598	64	8±2	26.2±1.8	—	Int.
GEMS_N7144_01B	KTS 65 A,B	21:44:53.7, -49:00:27.7	1586	81	12±2	26.2±1.8	—	Int.
GEMS_N7144_05	B215242.56-492853.8*	21:55:56.8, -49:14:37.3	1849	81	2.8±0.1	5.9±0.8	—	—
GEMS_N7144_06A	ESO 236-G036	21:42:52.9, -47:51:22.8	2004	77	1.9±0.1	24.8±1.5	—	IB(s)m
GEMS_N7144_06B	ESO 236-G035	21:42:48.3, -47:59:05.1	1958	168	2.5±0.1	24.8±1.5	2086	SB(rs)c
GEMS_N7144_07	B213743.74-4654387*	21:41:07.1, -46:38:50.1	1939	31	0.7±0.1	3.0±0.57	—	—
GEMS_HCG90_11A	NGC 7204	22:06:53.2, -31:03:07.1	2542	178	2.5±0.1	23.0±2.3	2630	S0/a pec.
GEMS_HCG90_11B	ESO 467-G002	22:06:09.9, -31:05:19.0	2583	40	1.6±0.1	23.0±2.3	2550	Sd

The columns are: (1) GEMS name, (2) Optical identification (* refers to the APMUKS(BJ) catalogue), (3) fitted H I center position, (4) observed H I systemic velocity, (5) 50% velocity width, (6) measured ATCA H I flux, (7) measured Parkes H I mass (from Kilborn et al. 2007). (8) optical velocity from NED, (9) morphological type from NED

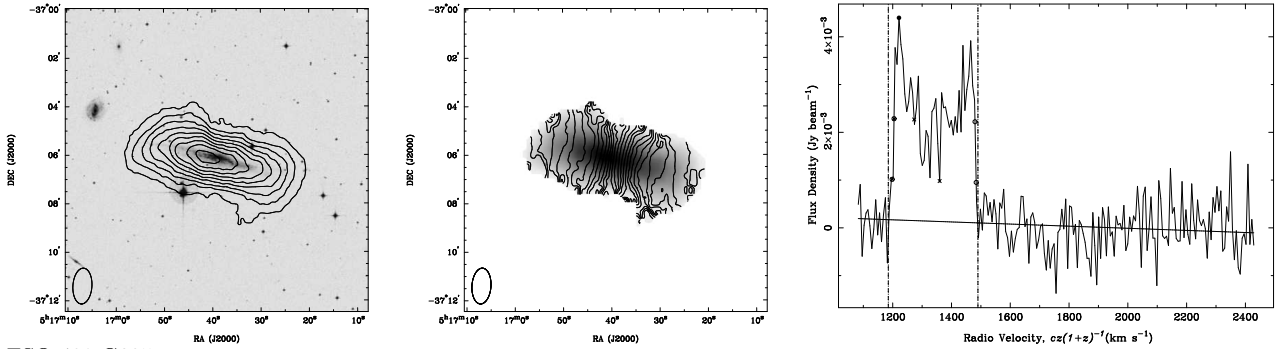
IC 1953



NGC 1385



ESO 362-G011



ESO 439-G025

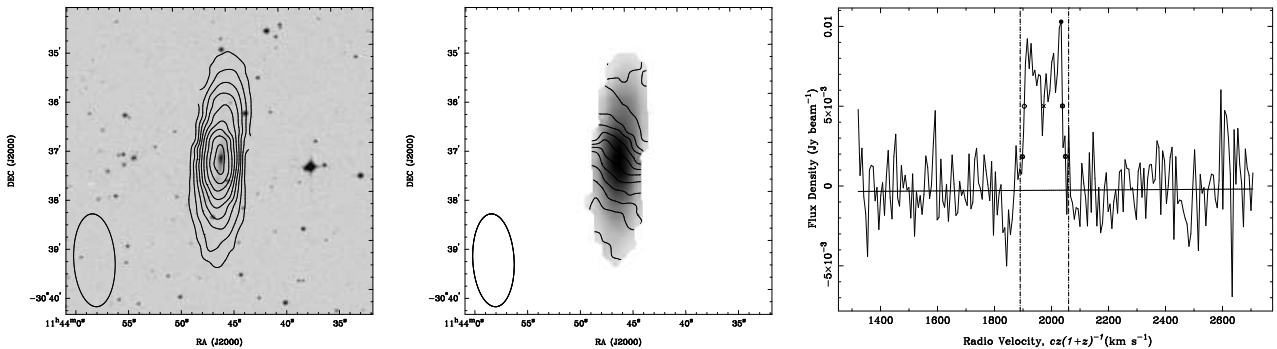


Figure 1. H I moment and spectral line maps of IC 1953, NGC 1385, ESO 362-G011, and ESO 439-G025, respectively, according to row. Column one shows the integrated H I intensity (contours) overlaid on an optical DSS image. The contour levels begin at $0.5 \text{ Jy beam}^{-1} \text{ km s}^{-1}$, and increment by $1.0 \text{ Jy beam}^{-1} \text{ km s}^{-1}$ for NGC 1385 and ESO 362-G011, and increment by $0.5 \text{ Jy beam}^{-1} \text{ km s}^{-1}$ for IC 1953 and ESO 439-G025. The second column shows the velocity contours over the H I integrated intensity greyscale, where the maps were masked below the $0.5 \text{ Jy beam}^{-1} \text{ km s}^{-1}$ level. The velocity increments are 10 km s^{-1} , with starting velocities at 1770, 1425, 1200, and 1920 km s^{-1} , respectively. The beam size is shown in the lower left of the H I line maps. Column three gives the H I spectra. The fitted baseline is shown, and the H I peak flux density is marked with a filled circle. The W_{20} and W_{50} velocity widths are shown by the open circles (outer fit), and crosses (inner fit). The velocity region between the vertical lines in the spectra was disregarded in the baseline fit.

with a uniform distribution. The velocity field is regular, and shows a slight change in the P.A. near the very edges of the H I emission. The H I spectrum is fairly symmetric. Although NED lists no optical redshift, an H I velocity was known previously from HIPASS (i.e. 1986 km s^{-1}). The Parkes H I source is resolved in our ATCA observations and is associated with the optical galaxy ESO 439-G025, which can now be confirmed as a member of the NGC 3923 group.

GEMS_N3923_11 is a previously uncatalogued low surface brightness, irregular galaxy as seen on the DSS (Figure 2). Its H I velocity and spatial location make it a new member of the NGC 3923 group. The H I is unresolved with an H I spectrum that shows a single central peak.

[**KK2000**] **47** has been previously catalogued by Karachentseva & Karachentsev (2000), who classified it as an Irr/Sph. There is no obvious nucleus nor spiral arms in the stellar component (Figure 2). The galaxy appears very diffuse, with low optical surface brightness. The H I is unresolved. The H I spectrum shows a central peak. Although NED lists no optical redshift, an H I velocity of $2125 \pm 2 \text{ km s}^{-1}$ was measured previously by Karachentseva & Karachentsev (2000) which places it in the NGC 3923 group.

3.4 NGC 5044 Group

LEDA 083818 This galaxy is classified as a late-type spiral. The H I distribution peaks on both sides of the galaxy (Figure 2). The H I spectrum is a symmetrical double horned profile. The GEMS redshift confirms it as a new member of the NGC 5044 group.

RC3 1303.0-1530 This galaxy is classified as a barred dwarf spiral. The H I has a regular distribution which is nearly centered on the bright nucleus of the galaxy (Figure 2). The velocity contours reveal a rotating disk, and the H I spectrum shows a central peak. The GEMS redshift confirms it as a new member of the NGC 5044 group.

[**MMB2004**] **J1320-1427** has been previously studied as part of our GEMS project by McKay et al. (2004), with the 750A array on the ATCA for a full 12 hour integration. The integrated H I flux as detected by McKay et al. (2004) is similar to the Parkes measurements (Kilborn et al. 2007). Our ATCA observations, taken in snapshot mode, did not recover the entire H I flux, but the spectra and corresponding H I integrated intensity map (Figure 3) are consistent with McKay et al. (2004). The spectrum is centrally peaked, and the integrated H I intensity shows an extension to the south-east, with most of the H I centered on two bright stellar components. McKay et al (2004) show that a deep R-band image reveals a faint halo around the two bluer and brighter regions visible in the DSS image.

RC3 1305.5-1430 The stellar component shows a distinct, but small nucleus, with an irregular shape (Figure 3). The H I component shows a peak at the optical nucleus, where the H I extends further south. The velocity field is unresolved, and the H I spectrum is asymmetric with more H I on the approaching side. The GEMS redshift confirms it as

a new member of the NGC 5044 group.

GEMS_N5044_18 is a previously uncatalogued very faint low surface brightness galaxy (Figure 3). Its H I velocity and spatial location make it a new member of the NGC 5044 group. The stellar component is sufficiently faint on the DSS that it can only be classified as an irregular galaxy. The H I is unresolved and the H I spectrum shows a single central peak.

3.5 NGC 7144 Group

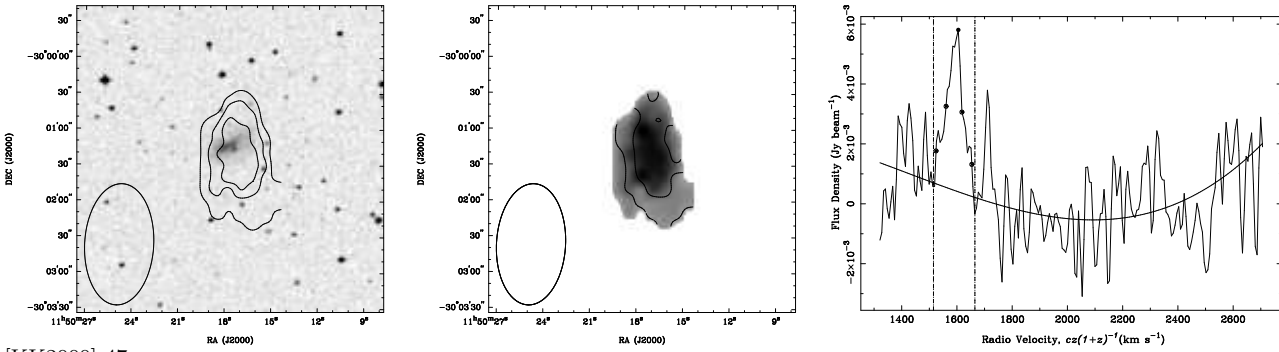
ESO 236-G039 and **KTS 65 A,B** This system consists of three irregular galaxies that are interacting. In Figure 4 our integrated H I map reveals a common H I envelope with peaks centred on ESO 236-G039 and between the two nuclei of KTS 65A,B with a bridge of H I connecting the three galaxies. The H I spectrum of ESO 236-G039 and KTS 65 A,B are both symmetric. The H I velocity map is irregular with some velocity substructure. The H I channel maps (Figure 5) show that the lower velocity H I gas is peaked between KTS 65 A,B, it extends smoothly in a bridge towards ESO 236-G039, and ends with the highest velocity gas peaked on ESO 236-G039. Given the projected separation of 2.75 kpc and a H I velocity difference of $\leq 12 \text{ km s}^{-1}$, the crossing time is $\sim 100 \text{ Myr}$. This suggests that the three galaxies will merge into a single merger-remnant galaxy on a short timescale. The fate of the H I gas will depend on how efficiently it is converted into stars, ionised or expelled from the system by supernovae.

[**APMUKS(BJ)**] **B215242.56-492853.8** This is a small, compact galaxy. The stellar component is slightly elongated along the same P.A. as the integrated H I (Figure 3). The H I is evenly distributed, extending much further out than the stellar counterpart. The velocity field shows regular rotation. The H I spectrum has a single central peak. Although NED lists no optical redshift, an H I velocity was known previously from the HIPASS survey (i.e. 1865 km s^{-1}) which is confirmed by our ATCA observations and hence we can assign it to the NGC 7144 group.

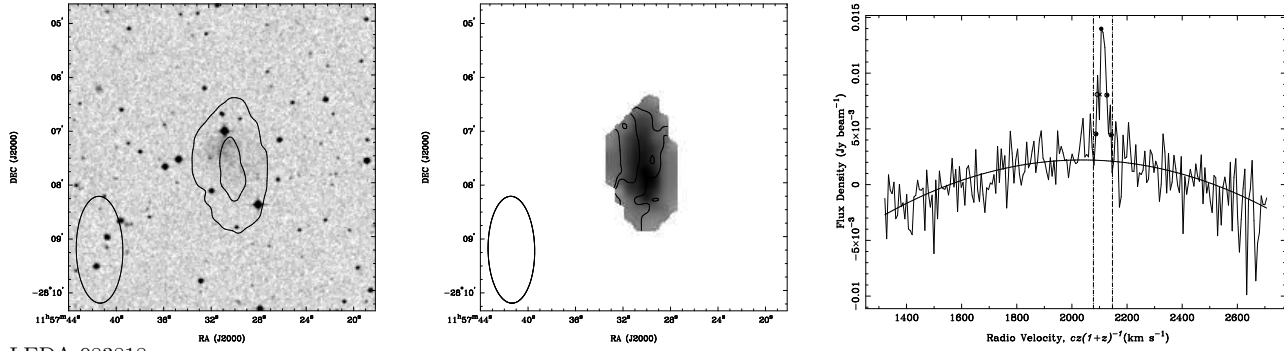
ESO 236-G036 is in an interacting pair with ESO 236-G035. The H I follows the stellar component in the north but extends beyond the optical galaxy to the south-west (Figure 6). This extended H I may be due to the interaction with ESO 236-G035. The H I map reveals several peaks. The velocity contours are regular and the H I spectrum is centrally peaked. We also note that the combined ATCA flux (3.4 Jy km s^{-1}) is less than that for the Parkes flux GEMS_N7144_6 (5.6 Jy km s^{-1}) suggesting additional H I may lie between the two galaxies. At a distance of 22.8 Mpc, this galaxy is separated by 52 kpc in projection from ESO 236-G035, and has a difference in velocity of 46 km s^{-1} .

ESO 236-G035 The H I distribution peaks at either side of the nucleus (Figure 6). The H I distribution shows a small extension to the south-west, perhaps due to an interaction with ESO 236-G036. The H I spectrum is asymmetric with most of the H I in the receding side, which is closer to ESO

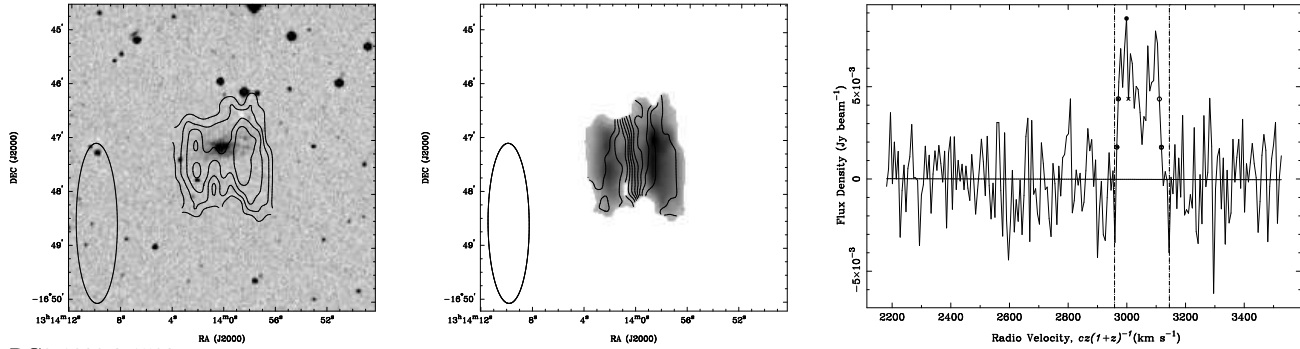
NGC 3923-11



[KK2000] 47



LEDA 083818



RC3 1303.0-1530

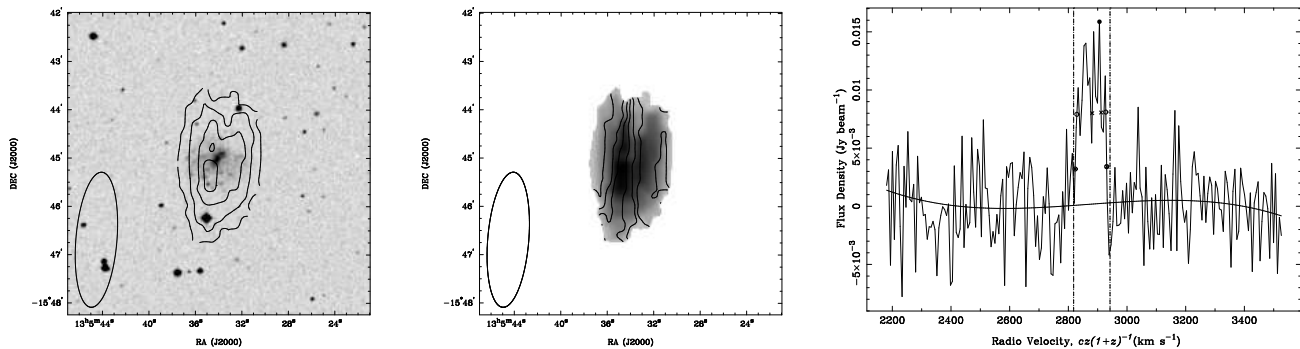
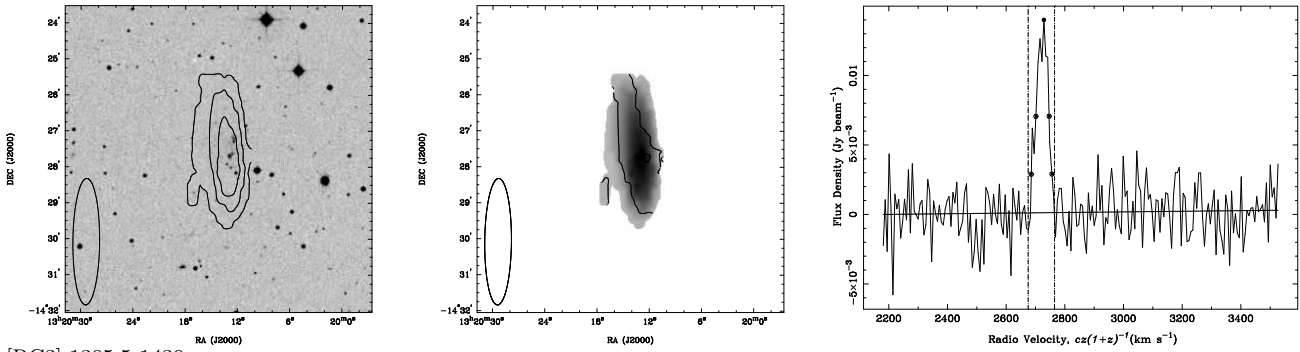
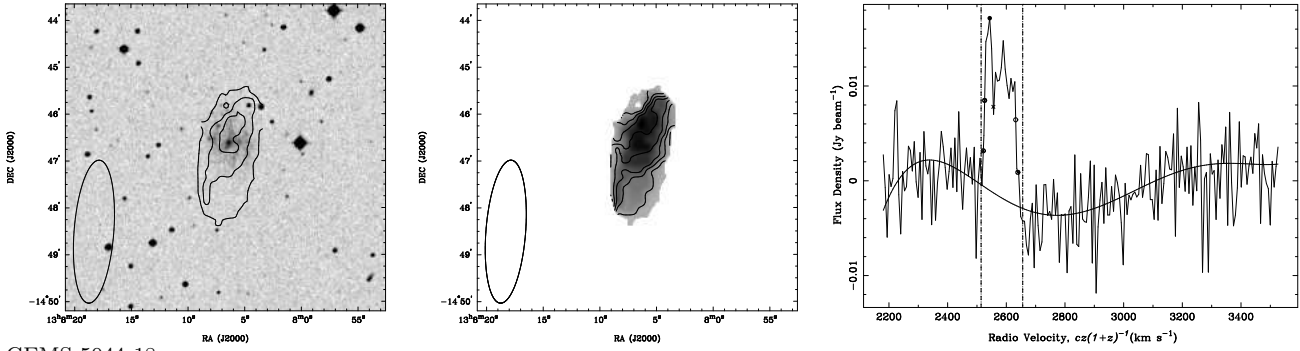


Figure 2. H I moment and spectral line maps of GEMS_N3923_11, [KK2000] 47, LEDA 083818, and RC3 1303.0-1530 respectively, according to row. Column one shows the integrated H I intensity (contours) overlaid on an optical DSS image. The contour levels for GEMS_N3923_11 and LEDA 083818, start at $0.3 \text{ Jy beam}^{-1} \text{ km s}^{-1}$, with increments of $0.2 \text{ Jy beam}^{-1} \text{ km s}^{-1}$. For all other galaxies, the contour levels begin at, and increment by, $0.5 \text{ Jy beam}^{-1} \text{ km s}^{-1}$. The beam is shown in the lower left of each figure. Column two gives the velocity contours over the H I integrated intensity greyscale, where the maps were masked below the $0.5 \text{ Jy beam}^{-1} \text{ km s}^{-1}$ level, except for GEMS_N3923_11 and LEDA 083818, where the maps were masked below $0.3 \text{ Jy beam}^{-1} \text{ km s}^{-1}$. The velocity increment for [KK2000] 47 is 2 km s^{-1} , where the rest have velocity increments of 10 km s^{-1} . Starting velocities are 2990, 2850, 1575, 2110 km s^{-1} , respectively. The beam size is shown in the lower left of the H I line maps. The third column shows the H I spectra. The spectrum of GEMS_N3923_11 was Hanning smoothed to a velocity resolution of 13.2 km s^{-1} . The fitted baseline is shown and the H I peak flux density is marked with a filled circle. The W_{20} and W_{50} velocity widths are shown by the open circles (outer fit), and crosses (inner fit). The velocity region between the vertical lines in the spectra were disregarded in the baseline fit.

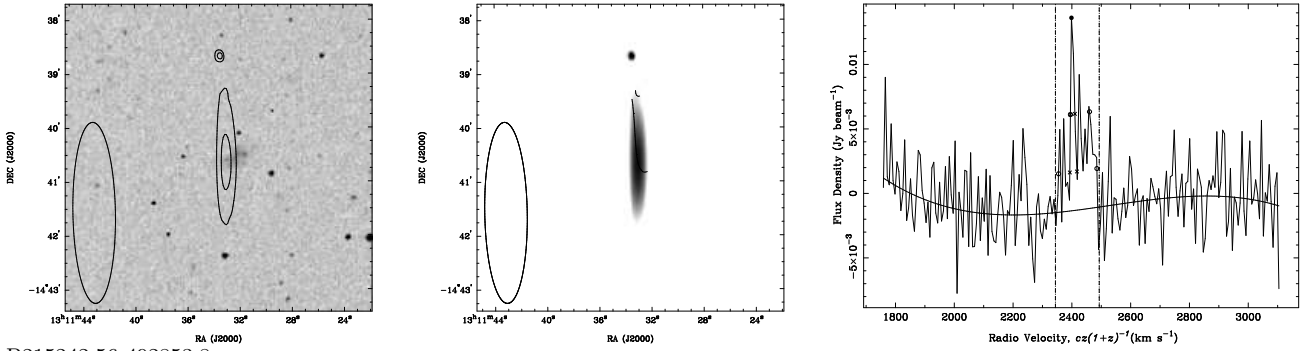
[MMB2004]J1320-1427



[RC3] 1305.5-1430



GEMS_5044_18



B215242.56-492853.8

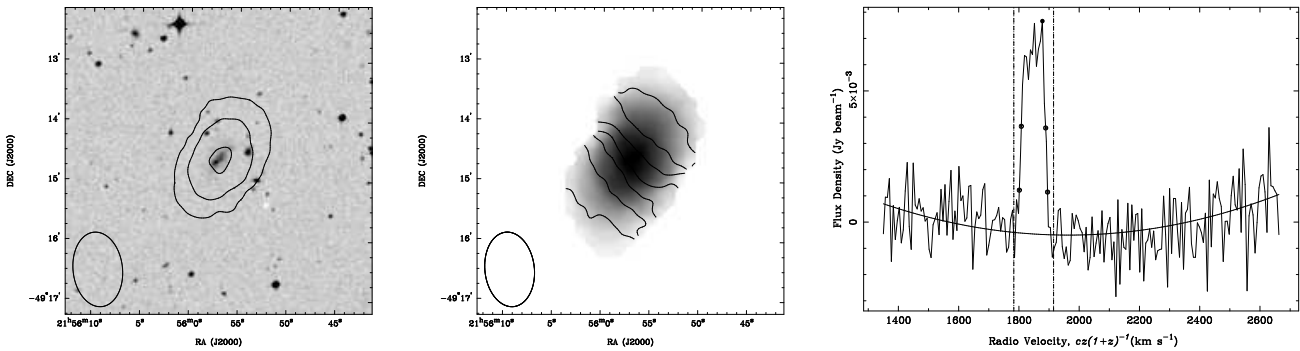


Figure 3. H I moment and spectral line maps of [MMB2004] J1320-1427, RC3 1305.5-1430, GEMS_N5044.18, and B215242.56-492853.8, respectively, according to row. Column one shows the integrated H I intensity (contours) overlaid on an optical DSS image. For GEMS_N5044.18, the contour levels begin at $0.28 \text{ Jy beam}^{-1} \text{ km s}^{-1}$, and increment by $0.04 \text{ Jy beam}^{-1} \text{ km s}^{-1}$. For all others, the contour levels begin at, and increment by, $0.5 \text{ Jy beam}^{-1} \text{ km s}^{-1}$. The second column shows the velocity contours over the H I integrated intensity greyscale, where the maps were masked below the first contour mentioned above. The velocity increments are 10 km s^{-1} , with starting velocities at 2718, 2540, 2402, 1817 km s^{-1} , respectively. The beam size is shown in the lower left of the H I line maps. Column three gives the H I spectra. The fitted baseline is shown, and the H I peak flux density is marked with a filled circle. The W_{20} and W_{50} velocity widths are shown by the open circles (outer fit), and crosses (inner fit). The velocity region between the vertical lines in the spectra were disregarded in the baseline fit.

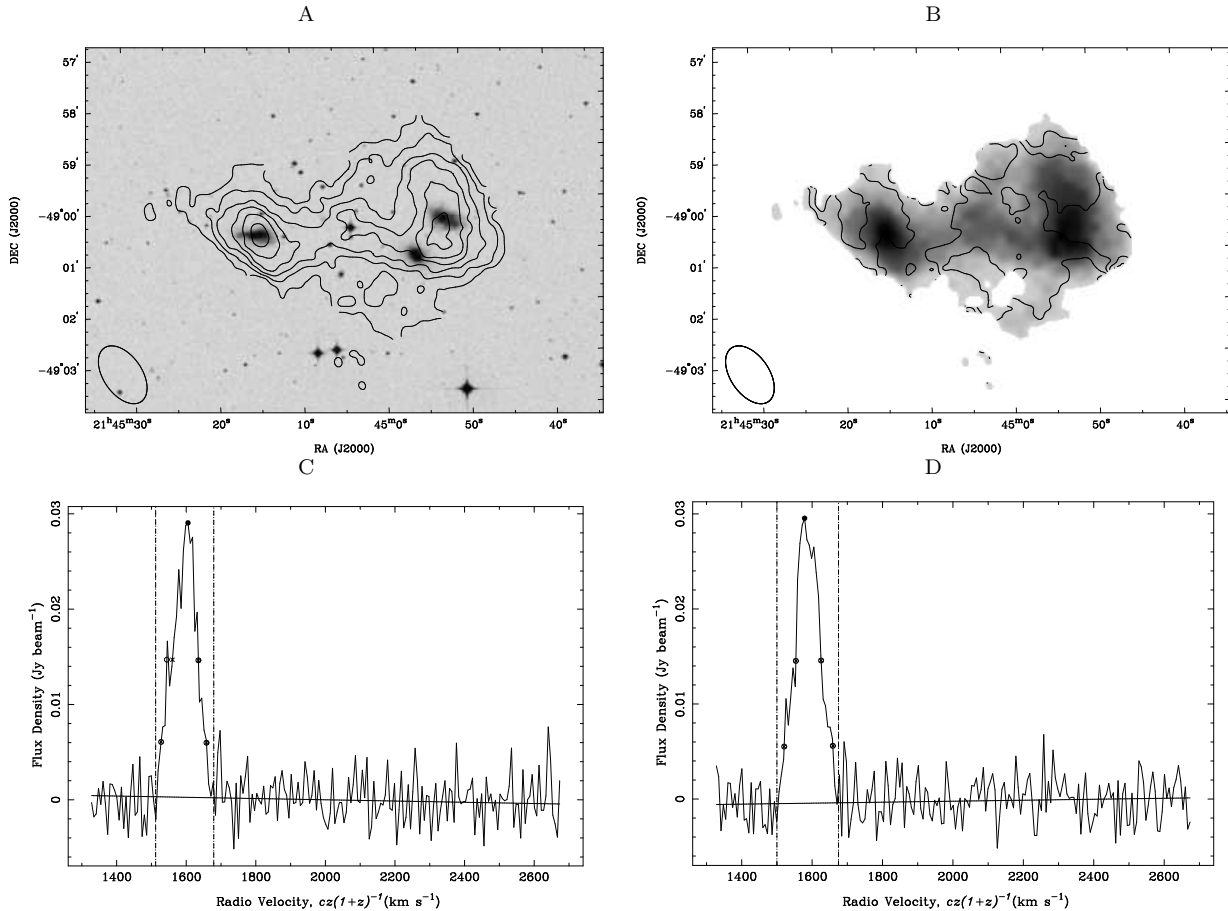


Figure 4. H I moment and spectral line maps of ESO 236-G039, and KTS 65 A&B. (A) The integrated H I intensity (contours) overlaid on an optical DSS image. The contour levels begin at $0.3 \text{ Jy beam}^{-1} \text{ km s}^{-1}$, and increment by $0.2 \text{ Jy beam}^{-1} \text{ km s}^{-1}$. (B) The velocity contours over the H I integrated intensity greyscale, where the map was masked below the $0.3 \text{ Jy beam}^{-1} \text{ km s}^{-1}$ level. The levels start at 1582 km s^{-1} , and increments by 8 km s^{-1} to 1606 km s^{-1} . The beam size is shown in the lower left of panels A and B. (C) The H I spectrum of ESO 236-G039. (D) The H I spectrum of KTS 65 A&B. Both spectra were Hanning smoothed to a velocity resolution of 13.2 km s^{-1} . The fitted baseline is shown, and the H I peak flux density is marked with a filled circle. The W_{20} and W_{50} velocity widths are shown by the open circles (outer fit), and crosses (inner fit). The velocity region between the vertical lines in the spectra were disregarded in the baseline fit.

236-G036.

[APMUKS(BJ)] **B213743.74-4654387** This is a small, compact galaxy (Figure 7). The stellar component lies entirely within the highest contour of the H I where the H I extends further to the west, and has an oblong shape. The velocity contours are regular across the disk, and the H I spectrum has a single central peak. The GEMS redshift confirms it as a new member of the NGC 7144 group.

3.6 HCG 90 Group

NGC 7204 This galaxy is actually a strongly interacting pair of galaxies. The H I peak is centered between the two galaxies (Figure 8). The eastern side of the H I does not extend past the stellar component, while the western side extends further out. The H I velocity field reveals a surprisingly regular rotation. NGC 7204 lies in a chain of galaxies with NGC 7201 and NGC 7203. Rubin (1974) present long-exposure image-tube photographs (shown in their paper in

Figure 2) of the galaxy chain. The Rubin image of NGC 7204 suggests a complex star formation and/or dust distribution.

ESO 467-G002 This is a blue, low surface-brightness galaxy (Roennback & Bergval 1994). The H I extends slightly further than the optical but is mostly unresolved by us (Figure 8). Roennback & Bergvall (1994) derive an optical inclination of $i = 63^\circ$, and a P.A. = 43° . The H I velocity field is regular, with a P.A. similar to the optical.

4 DISCUSSION AND CONCLUSIONS

We have followed up, at higher spatial resolution with the ATCA, sixteen H I sources in 6 southern GEMS groups that were previously detected by the Parkes telescope for which the optical counterpart was not clearly identified (due to the large beamsizes of the Parkes telescope). The superior spatial resolution of the ATCA allows us to clearly identify

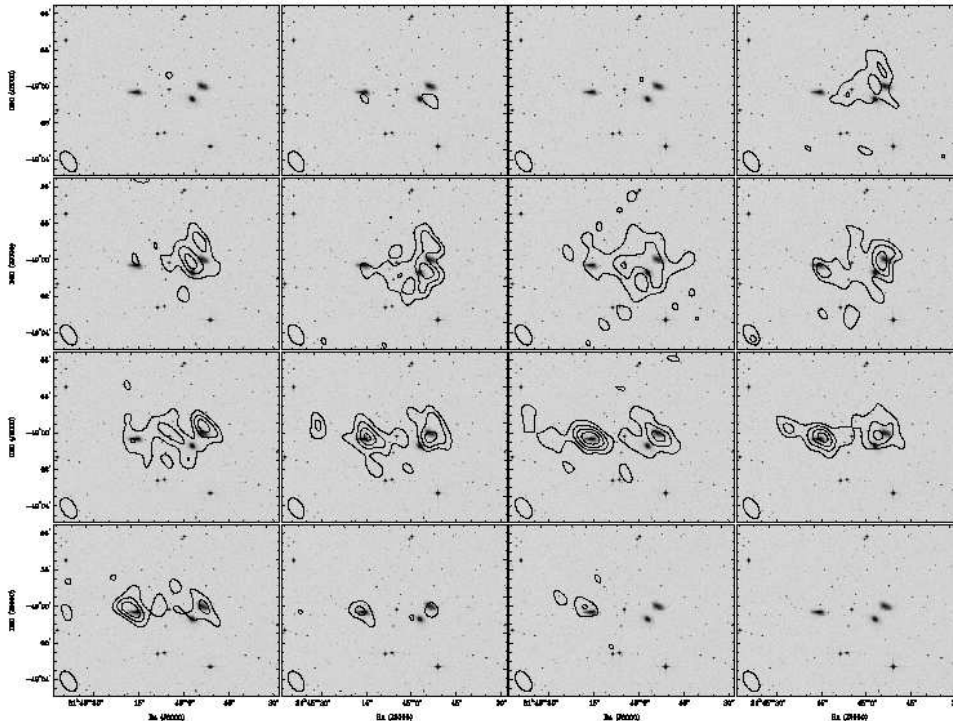


Figure 5. Channel maps of ESO 236-G039 (left) and KTS 65 A&B (right), overlaid on a DSS map. The panels step in velocity from left to right, then top to bottom. The contours begin at $0.028 \text{ Jy beam}^{-1} \text{ km s}^{-1}$, and increment by $0.01 \text{ Jy beam}^{-1} \text{ km s}^{-1}$. The beamsize is shown lower left.

an optical counterpart in each case. We find a variety of H I structures and velocity fields. These optical counterparts are mostly low surface brightness late-type galaxies, some are clearly tidally interacting galaxies.

Three Parkes sources are clearly associated multiple optical counterparts. The Parkes source GEMS_HCG90_11 is resolved into H I associated with NGC 7204 and ESO 467-G002. There is no sign of an interaction between them, however we note that NGC 7204 itself is a strongly interacting close pair of galaxies. Two Parkes sources in the NGC 7144 group appear to be associated with interacting systems. Optical counterparts KTS 65 A&B and ESO 236-G039 are in an interacting system, which reveals a bridge of H I within a common H I envelope. We suggest it will merge into a single gas-rich galaxy on a ~ 100 Myr timescale. The second Parkes source in this group is associated with ESO 236-G035 and ESO 236-G036. The H I contours of both galaxies are roughly aligned with each other. Thus they may also form an interacting system with a relative velocity of only 46 km s^{-1} between them. Interestingly, a friends-of-friends analysis indicates that the NGC 7144 group has yet to form a coherent group structure and may be an example of a group that is still collapsing (Brough et al. 2006).

We find no obvious cases for ram pressure stripping in the H I structures. Most galaxies are at projected radii in the outskirts of the groups, where any intragroup medium would be minimal. When irregular, extended H I structures were seen they tended to be in interacting systems. Kilborn et al. (2007) measured the H I deficiency of the Parkes sources in our 6 groups and 10 other GEMS groups, con-

cluding that ram pressure stripping was not the dominant process in removing H I gas.

For two of the H I sources (GEMS_N3923_11 and GEMS_N5044_18) we have succeeded in identifying previously uncatalogued optical counterparts. In both cases, the optical galaxies appear as faint, low surface brightness objects on the DSS. The H I velocity, and spatial location, of these galaxies indicates that they are new members of the NGC 3923 and NGC 5044 groups. We have also confirmed six new group members in the NGC 3923, 5044 and 7144 groups.

Deeper H I observations will no doubt reveal additional group members and hence further populate the dwarf end of the group mass (and optical luminosity) function. The recent very deep H I observations of Morganti et al. (2006) indicate that the H I mass function has a very long tail to low H I masses. This suggests that more dwarf galaxies in groups await discovery with future deep H I observations.

ACKNOWLEDGMENTS

We thank Enno Middelberg for help with the ATCA H I observing. We also thank the Australian Research Council for financial support.

This research has made extensive use of the NASA/IPAC Extragalactic Database (NED) which is operated by the Jet Propulsion Laboratory, Caltech, under contract with the National Aeronautics and Space Administration. The Digitized Sky Survey (DSS) was produced by

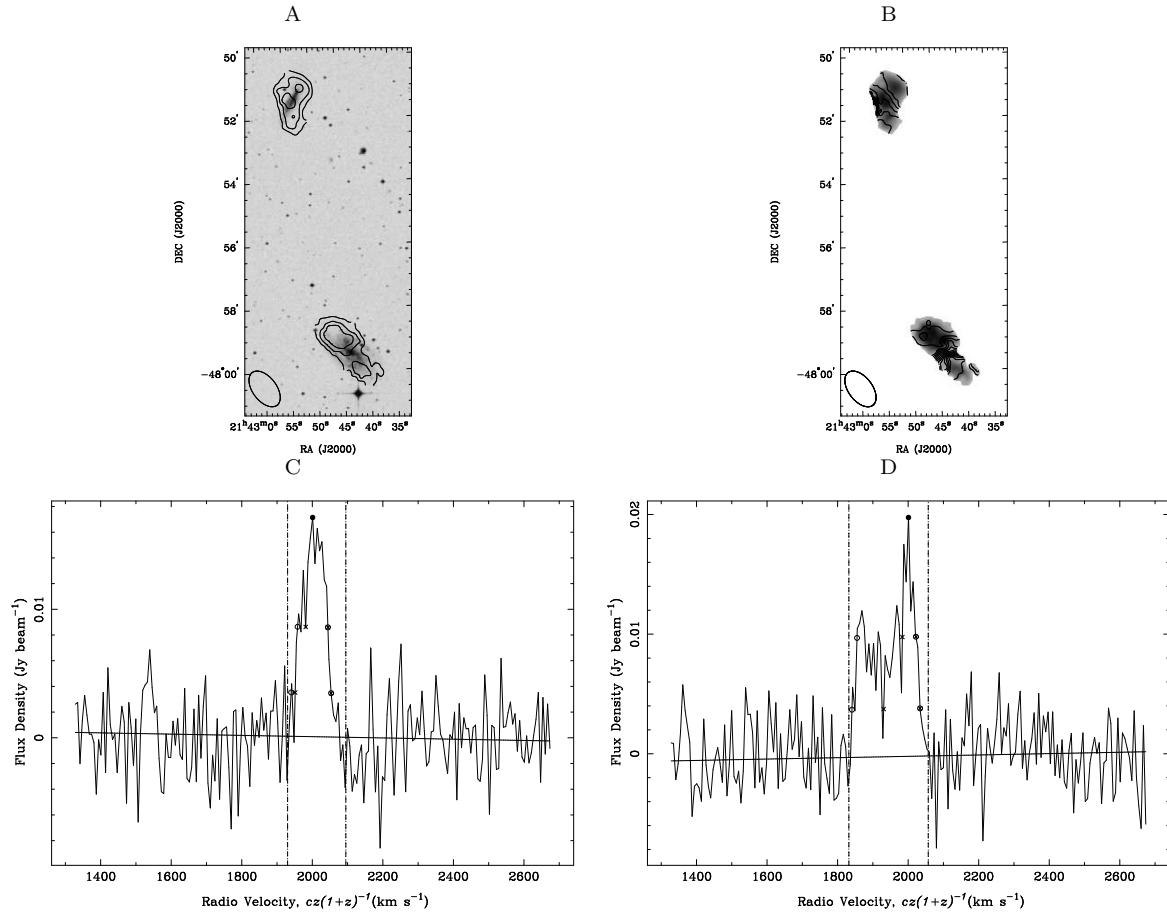


Figure 6. H I moment and spectral line maps of ESO 236-G036 and ESO 236-G035. ESO 236-G036 and ESO 236-G035 are mapped together due to their small angular separation, where ESO 236-G036 is at the top, and ESO 236-G035 is on the bottom. (A) The integrated H I intensity (contours) overlaid on an optical DSS image. The contour levels begin at, and increment by, $0.5 \text{ Jy beam}^{-1} \text{ km s}^{-1}$. (B) The velocity contours over the H I integrated intensity greyscale, where the maps were masked below the $0.5 \text{ Jy beam}^{-1} \text{ km s}^{-1}$ level. The velocity increments are 10 km s^{-1} , with a starting velocity of 1865 km s^{-1} . The beam size is shown in the lower left of panels A and B. (C) The H I spectra of ESO 236-G036. (D) The H I spectra for ESO 236-G035. The fitted baseline is shown, and the H I peak flux density is marked with a filled circle. The W_{20} and W_{50} velocity widths are shown by the open circles (outer fit), and crosses (inner fit). The velocity region between the vertical lines in the spectra were disregarded in the baseline fit.

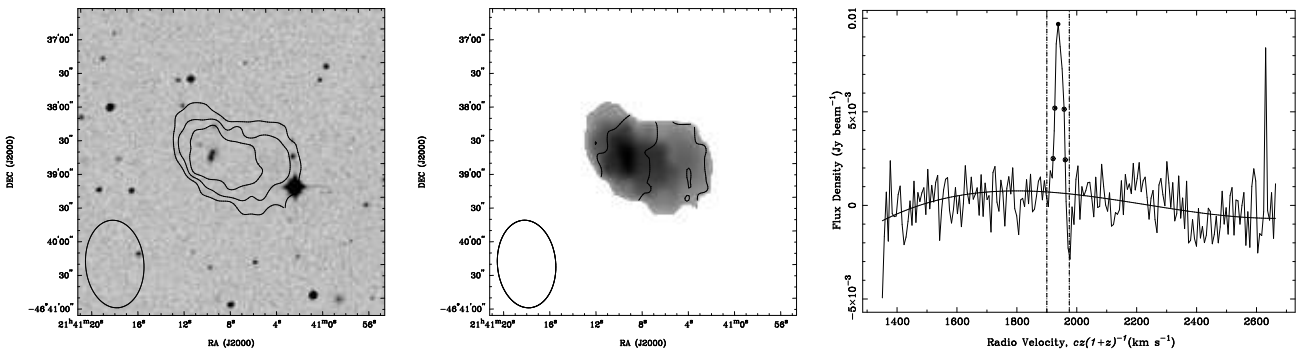


Figure 7. H I moment and spectral line maps of B213743.74-4654387. Column one gives the integrated H I intensity (contours) overlaid on an optical DSS image. The contour levels begin at $0.3 \text{ Jy beam}^{-1} \text{ km s}^{-1}$ and increment by $0.1 \text{ Jy beam}^{-1} \text{ km s}^{-1}$. Column two gives the the velocity contours over the H I integrated intensity greyscale, where the maps were masked below the $0.3 \text{ Jy beam}^{-1} \text{ km s}^{-1}$ level. The velocity increments are 10 km s^{-1} , with a starting velocity of 1934 km s^{-1} . The beam size is shown in the lower left of the H I line maps. Column 3 gives the H I spectrum. The fitted baseline is shown, and the H I peak flux density is marked with a filled circle. The W_{20} and W_{50} velocity widths are shown by the open circles (outer fit), and crosses (inner fit). The velocity region between the vertical lines in the spectra were disregarded in the baseline fit.

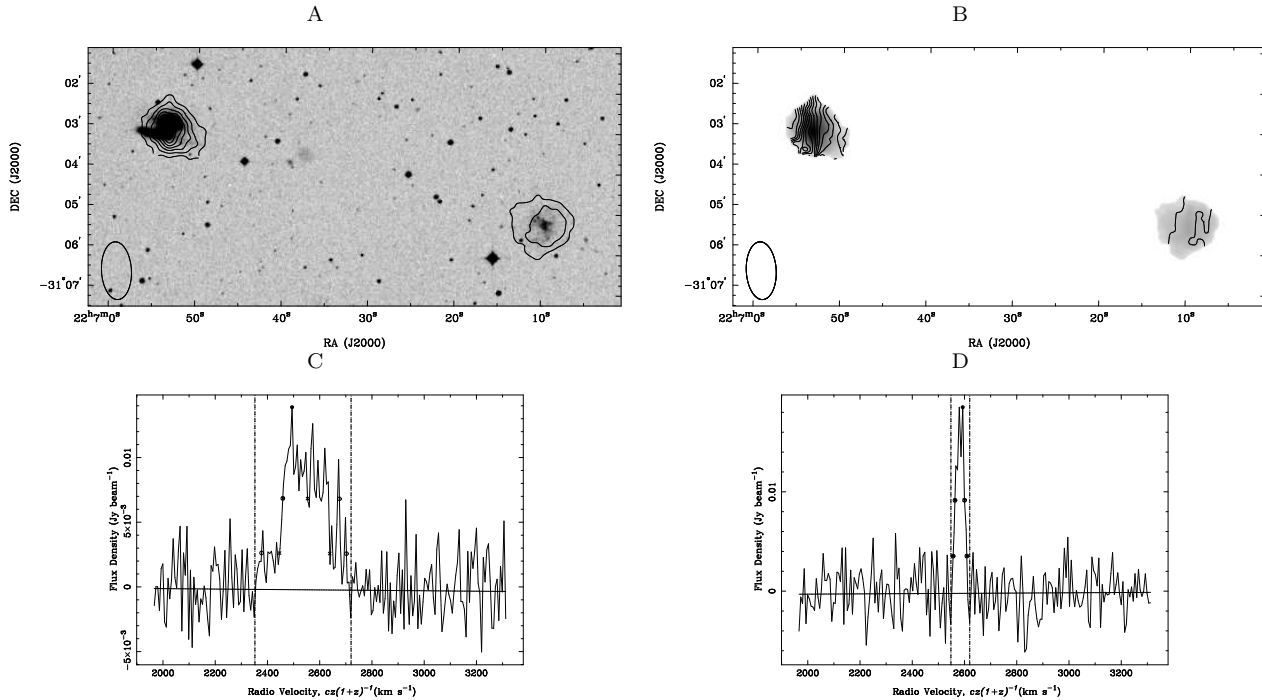


Figure 8. HI moment and spectral line maps of NGC 7204 and ESO 467-G002, where NGC 7204 is to the left of the maps, and ESO 467-G002 is to the right. (A) The integrated HI intensity (contours) overlaid on an optical DSS image. The contour levels begin at, and increment by, $0.5 \text{ Jy beam}^{-1} \text{ km s}^{-1}$. (B) Shows the velocity contours overlaid on the HI integrated intensity greyscale. The velocity increments are 10 km s^{-1} , with starting velocity of 2480 km s^{-1} . The beam size is shown in the lower left of panels A and B. (C) The HI spectra of NGC 7204. (D) gives the HI spectra of ESO 467-G002. The fitted baseline is shown, and the HI peak flux density is marked with a filled circle. The W_{20} and W_{50} velocity widths are shown by the open circles (outer fit), and crosses (inner fit). The velocity region between the vertical lines in the spectra were disregarded in the baseline fit.

the Space Telescope Science Institute (STScI) and is based on photographic data from the UK Schmidt Telescope, the Royal Observatory Edinburgh, the UK Science and Engineering Research Council, and the Anglo-Australian Observatory.

Roemback, J., Bergval, N., 1994, *A&AS*, 108, 193
 Rubin, V. C., 1974, *ApJ*, 191, 645
 Stevens, J., et al. 2004, *PASP*, 21, 318
 Wilman D. J., et al., 2005a, *MNRAS*, 358, L11
 Wilman D. J., et al., 2005b, *MNRAS*, 358, 88
 Verdes-Montenegro, L., et al. 2001, *A&A*, 377, 812

REFERENCES

- Barnes, D., et al. 2001, *MNRAS*, 322, 486
 Broeils A. H., van Woerden H., 1994, *A&AS*, 107, 129
 Brough, S., Forbes, D. A., Kilborn, V. A., Couch, W., 2006, *MNRAS*, 370, 1223
 Eke V. R., et al., 2004, *MNRAS*, 348, 866
 Forbes, D. A., et al. 2006, *PASA*, 23, 38
 Gordon S., Koribalski B., Jones K., 2003, *MNRAS*, 342, 939
 Kantharia, N. G., Ananthakrishnan, S., Nityananda, R., Hota, A., 2005, *A&A*, 435, 483
 Karachentseva, V. E., Karachentsev, I. D., 2000, *A&AS*, 146, 359
 Kilborn V. A., Koribalski B. S., Forbes D. A., Barnes D. G., Musgrave R. C., 2005, *MNRAS*, 356, 77
 Kilborn, V. A., et al., 2007, *MNRAS*, in prep.
 Koribalski, B., Manthey, E., 2005, *MNRAS*, 358, 202
 Mamon, G., 2006, *astro-ph/0607482*
 Martin, P., 1995, *AJ*, 109, 2428
 McKay, N. P. F., et al., 2004, *MNRAS*, 352, 1121
 Morganti, R., et al. 2006, *MNRAS*, 371, 157
 Mulchaey J. S., Zabludoff A. I., 1998, *ApJ*, 496, 73
 Neff, S. G., et al., 2005, *ApJ*, 619, 91
 Osmond J. P., Ponman T. J., 2004, *MNRAS*, 350, 1511
 Rasmussen, J., Ponman, T., Mulchaey, J., 2006, *MNRAS*, 370, 453